SUPPLEMENTARY INFORMATION

Femtosecond Fluorescence and Intersystem Crossing in Rhenium(I) Carbonyl-Bipyridine Complexes

Andrea Cannizzo,[a] Ana Maria Blanco-Rodríguez,[b] Amal El Nahhas,[a] Jakub Šebera,[c]

Stanislav Záliš,[c] Antonín Vlček, Jr.,*[b,c] Majed Chergui*[a]*

[a] *Laboratoire de Spectroscopie Ultrarapide, ISIC, FSB-BSP, Ecole Polytechnique Fédérale de Lausanne, CH-1015 Lausanne-Dorigny, Switzerland*
[b] *School of Biological and Chemical Sciences, Queen Mary, University of London, Mile End Road, London E1 4NS, United Kingdom*
[c] *J. Heyrovský Institute of Physical Chemistry, Academy of Sciences of the Czech Republic, Dolejškova 3, CZ-182 23 Prague, Czech Republic*
e-mail: Majed.Chergui@epfl.ch, a.vlcek@qmul.ac.uk, stanislav.zalis@jh-inst.cas.cz

I. STEADY STATE UV-VIS ABSORPTION SPECTRA AND CALCULATED TRANSITION STRENGTHS:

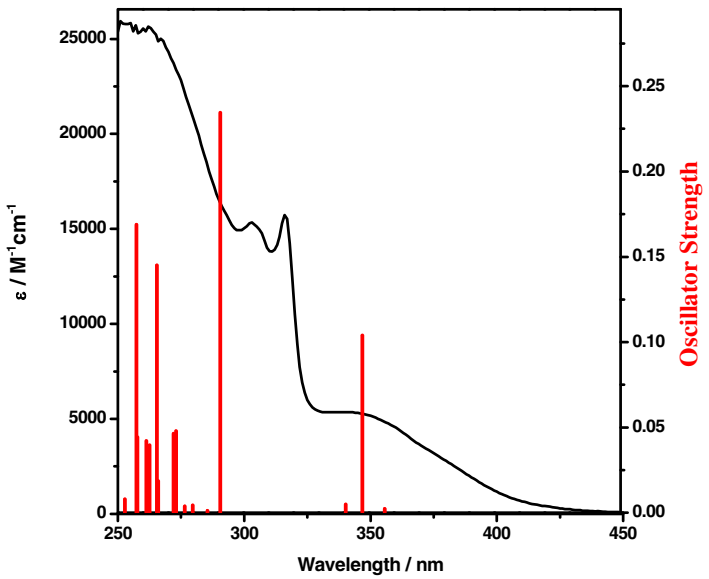

Figure S1. UV-vis absorption spectrum of $[Re(Etpy)(CO)_3(bpy)]^+$ in CH_3CN, shown together with TD-DFT (PBE0, CPCM for CH_3CN) calculated electronic transitions of $[Re(py)(CO)_3(bpy)]^+$ (red bars, calculated oscillator strengths shown on the right).

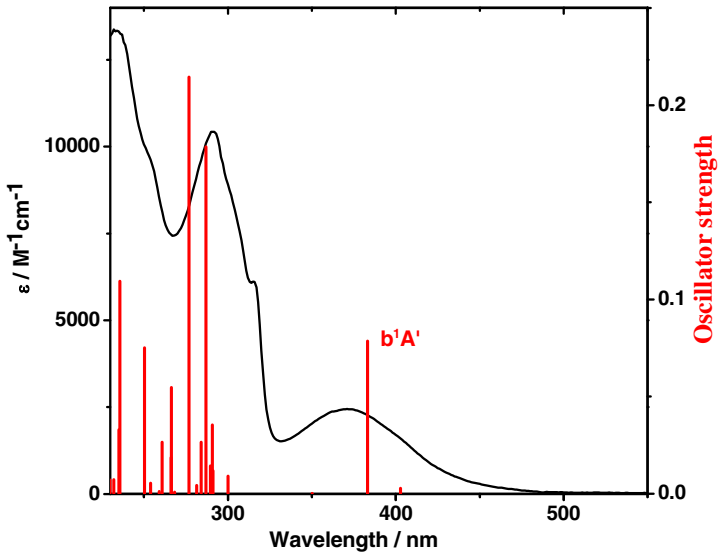

Figure S2. UV-vis absorption spectrum of [Re(Cl)(CO)$_3$(bpy)] in CH_3CN, shown together with TD-DFT (PBE0, CPCM for CH_3CN) calculated electronic transitions (red bars, calculated oscillator strengths shown on the right).

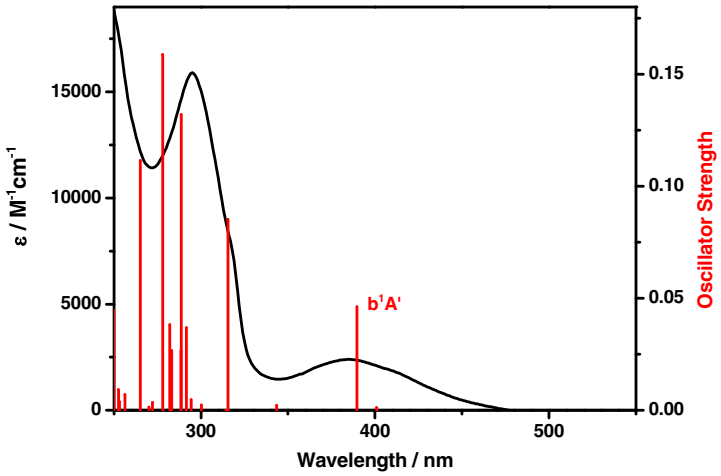

Figure S3. UV-vis absorption spectrum of [Re(I)(CO)$_3$(bpy)] in CH_3CN, shown together with TD-DFT (PBE0, CPCM for CH_3CN) calculated electronic transitions (red bars, calculated oscillator strengths shown on the right).

II. FLUORESCENCE UP-CONVERSION MEASUREMENTS: LUMINESCENCE SPECTRA AND TIME TRACES:

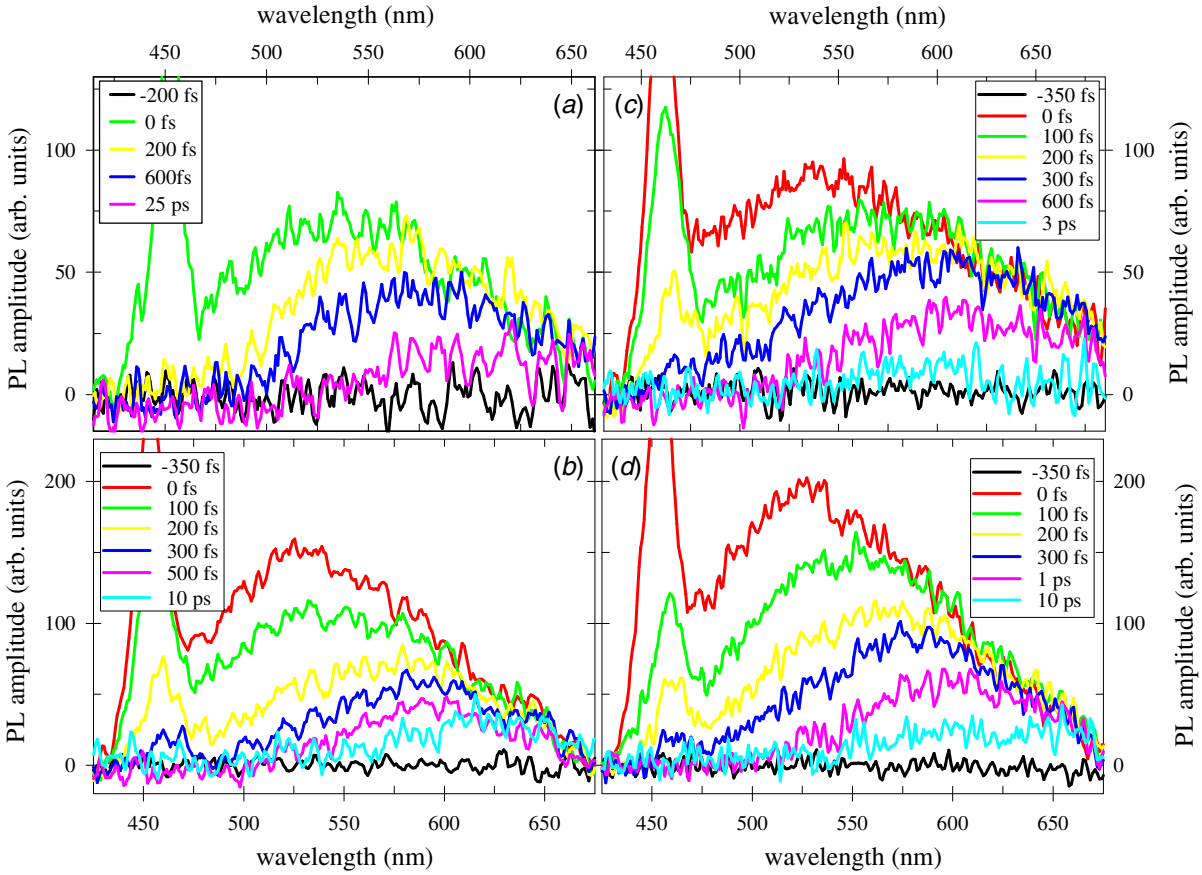

Figure S4. Luminescence spectra of $[Re(L)(CO)_3(bpy)]^n$ in CH_3CN, measured at selected time delays after 400 nm, ~80 fs excitation. (a): L = Etpy; (b): L = Cl; (c): L = Br, (d): L = I. The signal at ~457 nm is the solvent Raman line.

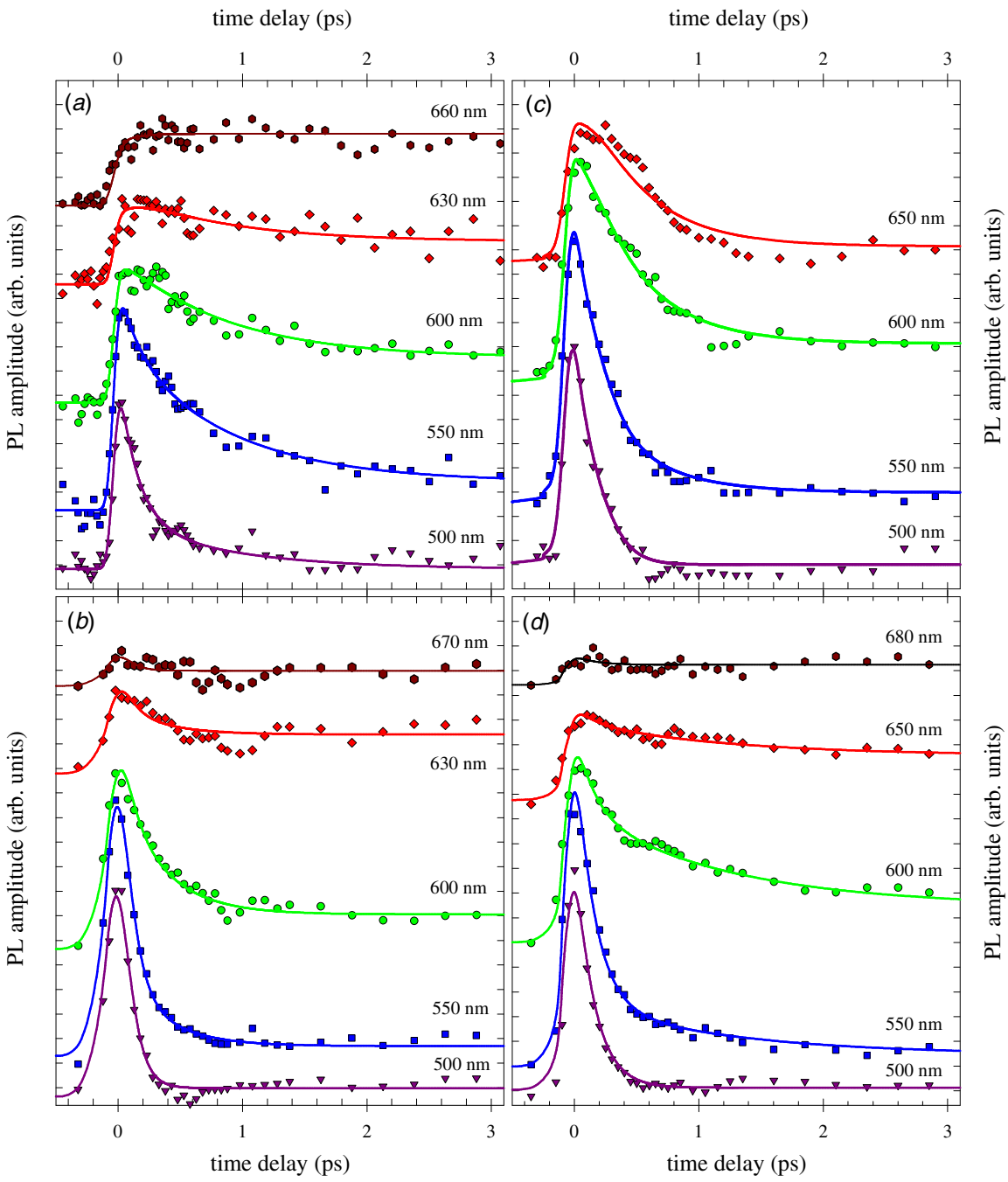

Figure S5. Time profiles at different luminescence wavelengths of $[Re(L)(CO)_3(bpy)]^n$ in CH_3CN, upon excitation with 400 nm, ~80 fs width pulses. (a): L = Etpy; (b): L = Cl; (c): L = Br, (d): L = I.

III. TABLES

Table S1. DFT (B3LYP/CPCM-CH_3CN) – calculated one-electron energies and compositions of spectroscopically relevant Kohn-Sham molecular orbitals of $[Re(py)(CO)_3(bpy)]^+$. Approximate symmetry within the C_s group is given in parenthesis. (Calculations in vacuum and CH_3CN give the same energy ordering of the orbitals and very similar compositions.)

MO	E (eV)	Prevailing character	Re	bpy	CO_{ax}	$2CO_{eq}$	py
Unoccupied	-						
94a (A")	-1.50	π* bpy	1	94	0	3	2
93a (A')	-1.59	π* bpy	2	66	2	2	28
92a (A')	-1.72	π* py	3	28	3	2	65
91a (A')	-2.66	π* bpy	3	92	0	4	1
Occupied							
90a (A")	-6.74	Re	61	8	11	14	6
89a (A')	-6.74	Re	64	8	13	13	1
88a (A')	-6.97	Re	68	2	1	28	1
87a (A")	-7.38	π bpy	1	99	0	0	0
86a (A")	-7.84	Py	1	0	0	0	99
85a (A')	-8.61	Py+bpy	1	27	0	1	72

Table S2. DFT (PBE0/CPCM-CH_3CN) – calculated one-electron energies and compositions of spectroscopically relevant Kohn-Sham molecular orbitals of $[Re(py)(CO)_3(bpy)]^+$. Approximate symmetry within the C_s group is given in parenthesis. (Calculations in vacuum and CH_3CN give the same energy ordering of the orbitals and very similar compositions.)

MO	E (eV)	Prevailing character	Re	bpy	CO_{ax}	$2CO_{eq}$	py
Unoccupied							
94a (A")	-1.42	π* bpy	1	94	0	3	2
93a (A')	-1.50	π* bpy	2	63	2	2	32
92a (A')	-1.65	π* py	2	32	3	2	61
91a (A')	-2.62	π* bpy	3	92	0	4	1
Occupied							
90a (A")	-7.07	Re	61	8	11	14	6
89a (A')	-7.07	Re	65	8	13	13	1
88a (A')	-7.31	Re	69	2	1	28	0
87a (A")	-7.69	π bpy	1	98	0	0	0
86a (A")	-8.15	Py	1	0	0	0	99
85a (A')	-8.94	Py+bpy	1	27	0	1	72

Table S3. DFT (B3LYP/CPCM-CH_3CN) – calculated one-electron energies and compositions of spectroscopically relevant Kohn-Sham molecular orbitals of [Re(Cl)$(CO)_3$(bpy)]. Approximate symmetry within the C_s group is given in parenthesis.

MO	E (eV)	Prevailing Character	Re	bpy	CO_{ax}	$2CO_{eq}$	Cl
Unoccupied							
82a (A")	-0.90	CO	25	6	14	55	1
81a (A")	-1.37	π* bpy	1	96	1	2	0
80a (A')	-1.55	π* bpy	1	96	0	2	0
79a (A')	-2.51	π* bpy	3	93	0	3	1
Occupied							
78a (A")	-6.19	Re + π Cl	53	3	15	11	18
77a (A')	-6.28	Re + π Cl	51	5	12	12	19
76a (A')	-6.67	Re	67	2	1	31	0
75a (A")	-7.25	π bpy	0	99	0	0	1
74a (A')	-7.71	Cl	12	16	1	3	68
73a (A")	-7.73	Cl	11	16	1	3	67

Table S4. DFT (PBE0/CPCM-CH_3CN) – calculated one-electron energies and compositions of spectroscopically relevant Kohn-Sham molecular orbitals of [Re(Cl)$(CO)_3$(bpy)]. Approximate symmetry within the C_s group is given in parenthesis.

MO	E (eV)	Prevailing character	Re	bpy	CO_{ax}	$2CO_{eq}$	Cl
Unoccupied							
82a (A")	-0.80	CO	26	6	13	54	1
81a (A")	-1.26	π* bpy	1	96	1	2	0
80a (A')	-1.45	π* bpy	1	96	0	2	0
79a (A')	-2.45	π* bpy	3	93	0	3	1
Occupied							
78a (A")	-6.55	Re + π Cl	53	3	15	11	18
77a (A')	-6.63	Re + π Cl	51	5	12	12	19
76a (A')	-7.02	Re	67	2	1	31	0
75a (A")	-7.53	π bpy	0	99	0	0	1
74a (A')	-8.01	Cl	11	15	1	2	70
73a (A")	-8.03	Cl	12	15	1	3	69

Table S5. DFT (B3LYP/CPCM-CH_3CN) calculated one-electron energies and compositions of spectroscopically relevant Kohn-Sham molecular orbitals of [Re(I)$(CO)_3$(bpy)]. Approximate symmetry within the C_s group is given in parenthesis.

MO	E (eV)	Prevailing character	Re	bpy	CO_{ax}	$2CO_{eq}$	I
Unoccupied							
100a (A")	-1.02	CO	28	6	15	51	0
99a (A")	-1.31	π* bpy	2	95	1	2	0
98a (A')	-1.47	π* bpy	3	91	0	4	2
97a (A')	-2.48	π* bpy	3	90	0	4	3
Occupied							
96a (A")	-6.16	π I + Re	32	2	9	6	51
95a (A')	-6.21	π I + Re	29	3	8	5	56
94a (A')	-6.74	Re	67	2	1	29	1
93a (A')	-6.94	π I + Re	27	12	5	5	50
92a (A")	-6.98	π I + Re	30	12	6	8	45
91a (A")	-7.22	π bpy	2	96	0	0	1

Table S6. DFT (PBE0/CPCM-CH_3CN) calculated one-electron energies and compositions of spectroscopically relevant Kohn-Sham molecular orbitals of [Re(I)$(CO)_3$(bpy)]. Approximate symmetry within the C_s group is given in parenthesis.

MO	E (eV)	Prevailing Character	Re	bpy	CO_{ax}	$2CO_{eq}$	I
Unoccupied							
100a (A")	-0.87	CO	28	6	15	51	0
99a (A")	-1.18	π* bpy	2	95	1	2	0
98a (A')	-1.36	π* bpy	3	91	0	4	2
97a (A')	-2.40	π* bpy	3	90	0	4	3
Occupied							
96a (A")	-6.42	π I + Re	32	2	9	6	51
95a (A')	-6.46	π I + Re	29	3	8	5	56
94a (A')	-7.03	Re	67	2	1	29	1
93a (A')	-7.22	π I + Re	27	12	5	5	50
92a (A")	-7.27	π I + Re	30	12	6	8	45
91a (A")	-7.49	π bpy	2	96	0	0	1

Table S7. TD-DFT G03/B3LYP/CPCM (ACN) calculated singlet electronic transitions of $[Re(L)(CO)_3(bpy)]^n$ with oscillator strength larger than 0.001. (Transition energies in eV, corresponding wavelength (nm) in parenthesis. Molar absorptivity in $M^{-1}cm^{-1}$)

State	Main components (%)	Calculated transitions	Osc. Str.	Expt. transitions	Molar abs.
$[Re(py)(CO)_3(bpy)]^+$					
a^1A“	97 (90a→91a)	3.31 (374)	0.002		
b^1A‘	93 (89a→91a); 6 (88a→91a)	3.38 (367)	0.095	3.65 (340)	5360
c^1A’	93 (88a→91a); 5 (89a→91a)	3.50 (354)	0.010		
b^1A”	85 (87a→91a)	4.16 (298)	0.189	3.92 (316)	15730
$[Re(Cl)(CO)_3(bpy)]$					
a^1A“	98 (78a→79a)	2.91 (426)	0.002		
b^1A‘	98 (77a→79a)	3.08 (403)	0.044	3.34 (371)	2450
e^1A‘	84 (78a→81a)	4.10 (302)	0.036		
c^1A”	72 (77a→82a); 12 (75a→79a)	4.19 (296)	0.030		
e^1A”	52 (75a→79a); 31 (77a→81a)	4.31 (287)	0.327	4.26 (291)	10430
$[Re(I)(CO)_3(bpy)]$					
a^1A“	99 (96a→97a)	2.98 (416)	0.002		
b^1A‘	99 (95a→97a)	3.08 (403)	0.044	3.23 (384)	2400
e^1A‘	98 (93a→97a)	3.80 (326)	0.073		
c^1A”	42 (95a→100a); 40 (91a→97a)	4.18 (296)	0.086		
e^1A”	45 (95a→99a); 40 (91a→97a)	4.32 (287)	0.234	4.20 (295)	15900

Table S8. TD-DFT G03/PBE0/CPCM (ACN) calculated singlet electronic transitions of $[Re(L)(CO)_3(bpy)]^n$ with oscillator strength larger than 0.001. (Transition energies in eV, corresponding wavelength (nm) in parenthesis. Molar absorptivity in $M^{-1}cm^{-1}$)

State	Main components (%)	Calculated transitions	Osc. Str.	Expt. transitions	Molar abs.
$[Re(py)(CO)_3(bpy)]^+$					
$a\,^1A''$	97 (90a→91a)	3.48 (356)	0.002		
$b\,^1A'$	92 (89a→91a); 6 (88a→91a)	3.57 (347)	0.101	3.65 (340)	5360
$c\,^1A'$	91 (88a→91a); 6 (89a→91a)	3.69 (336)	0.010		
$b\,^1A''$	77 (87a→91a)	4.27 (290)	0.259	3.92 (316)	15730
$[Re(Cl)(CO)_3(bpy)]$					
$a\,^1A''$	98 (78a→79a)	3.12 (397)	0.003		
$b\,^1A'$	97 (77a→79a)	3.28 (378)	0.080	3.34 (371)	2450
$e\,^1A'$	79 (78a→81a)	4.16 (298)	0.022		
$c\,^1A''$	50 (77a→82a); 26 (75a→79a)	4.29 (289)	0.081		
$e\,^1A''$	31 (75a→79a); 52 (77a→81a)	4.34 (286)	0.143	4.26 (291)	10430
$[Re(I)(CO)_3(bpy)]$					
$a\,^1A''$	99 (96a→97a)	3.09 (401)	0.002		
$b\,^1A'$	99 (95a→97a)	3.18 (389)	0.046	3.23 (384)	2400
$e\,^1A'$	98 (93a→97a)	3.93 (316)	0.085		
$c\,^1A''$	60 (95a→100a); 20 (91a→97a)	4.25 (292)	0.037		
$e\,^1A''$	40 (95a→100a); 45 (91a→97a)	4.30 (289)	0.132	4.20 (295)	15900

Table S9. Low-lying triplet electronic transitions of $[Re(L)(CO)_3(bpy)]^n$ calculated by TD-DFT (B3LYP, CPCM for CH_3CN).

State	Main components (%)	Transition energy (eV)
$[Re(py)(CO)_3(bpy)]^+$ in CH_3CN		
a ^{3}A"	48 (90a→91a); 45 (87a→91a)	2.85
a ^{3}A'	98 (89a →91a)	3.29
b ^{3}A"	53 (90a→91a); 47 (87a→91a)	3.31
$[Re(py)(CO)_3(bpy)]^+$ in vacuum		
a ^{3}A"	86 (90a→91a); 9 (87a→91a)	2.65
a ^{3}A'	98 (89a →91a)	2.97
b ^{3}A"	79 (87a→91a); 9 (90a→91a);	3.16
$[Re(Cl)(CO)_3(bpy)]$ in CH_3CN		
a ^{3}A"	82 (78a→79a); 16 (75a→79a)	2.77
a ^{3}A'	99 (77a→79a)	2.89
b ^{3}A"	75 (75a→79a); 15 (78a→79a)	3.13
$[Re(I)(CO)_3(bpy)]$ in CH_3CN		
a ^{3}A"	78 (96a→97a); 12 (91a→97a)	2.83
a ^{3}A'	96 (95a→97a)	2.93
b ^{3}A"	56 (91a→97a); 16 (96a→97a)	3.11

Table S10. Low-lying triplet electronic transitions of $[Re(L)(CO)_3(bpy)]^n$ calculated by TD-DFT (PBE0, CPCM for CH_3CN).

State	Main components (%)	Transition energy (eV)
$[Re(py)(CO)_3(bpy)]^+$ in CH_3CN		
a ^{3}A"	31 (90a→91a); 48 (87a→91a);	2.86
a ^{3}A'	96 (89a→91a)	3.30
b ^{3}A"	61 (90a→91a); 38 (87a→91a)	3.32
$[Re(py)(CO)_3(bpy)]^+$ in vacuum		
a ^{3}A"	63 (90a→91a); 24 (87a→91a);	2.70
a ^{3}A'	98 (89a→91a)	2.82
b ^{3}A"	26 (90a→91a); 62 (87a→91a)	3.14
$[Re(Cl)(CO)_3(bpy)]$ in CH_3CN		
a ^{3}A"	43 (78a→79a); 39 (75a→79a); 8 (75a→80a)	2.82
a ^{3}A'	97 (77a→79a)	3.05
b ^{3}A"	44 (78a→79a); 47 (75a→79a); 6 (75a→80a)	3.16
$[Re(I)(CO)_3(bpy)]$ in CH_3CN		
a ^{3}A"	35 (96a→97a); 29 (91a→97a); 11 (92a→97a)	2.83
a ^{3}A'	95 (95a→97a)	3.00
b ^{3}A"	49 (96a→97a); 34 (91a→97a); 7 (92a→97a)	3.11

Table S11. Selected TD-DFT (PBE0) calculated structural parameters of the a^1A' (ground), b^1A' and a^3A'' states of $[Re(Cl)(CO)_3(bpy)]$ and $[Re(py)(CO)_3(bpy)]^+$. %(S-GS) and %(T-S) are the percent change in the given parameter between the b^1A' and a^1A' states and the b^1A' and a^3A'' states, respectively.

	$[Re(Cl)(CO)_3(bpy)]$ in CH_3CN (COSMO)					$[Re(py)(CO)_3(bpy)]^+$ in vacuum				
Bond lengths, Å	a^1A'	b^1A'	%(S-G)	a^3A''	%(T-S)	a^1A'	b^1A'	%(G-S)	a^3A''	%(T-S)
Re-N	2.204	2.180	-1.1	2.147	-1.5	2.203	2.177	-1.2	2.135	-1.9
Re-L	2.499	2.426	-2.9	2.426	0.0	2.254	2.218	-1.6	2.225	0.1
Re-C_{ax}	1.925	1.960	1.8	1.972	0.6	1.947	1.976	1.5	1.992	0.8
Re-C_{eq}	1.933	1.965	1.7	1.968	0.2	1.942	1.987	2.3	1.977	-0.5
N-C6	1.337	1.340	0.2	1.346	0.4	1.341	1.343	0.1	1.347	0.3
N-C2	1.350	1.382	2.4	1.392	0.7	1.353	1.382	2.1	1.402	1.4
C2-C2’	1.476	1.433	-2.9	1.421	-0.8	1.477	1.433	-3.0	1.415	-1.3
C-O_{ax}	1.156	1.146	-0.9	1.145	-0.1	1.146	1.138	-0.7	1.138	0
C-O_{eq}	1.153	1.148	-0.4	1.147	-0.1	1.148	1.141	-0.6	1.143	0.2
Angles, °										
N1-Re-N2	74.3	76.4	2.8	77.0	0.8	74.4	77.1	3.6	77.7	0.8
Ceq-Re-Ceq	89.1	95.6	7.3	85.8	-10.3	89.7	94.5	5.4	85.5	-9.5
L-Re-Cax	175.2	178.9	2.1	174.6	-2.4	177.6	178.0	0.2	174.8	-1.8
N-Re-L	82.7	88.7	7.3	87.9	-0.9	85.6	85.5	-0.1	85.1	-0.5
N-Re-Cax	93.5	92.2	-1.4	88.0	-4.6	92.5	92.9	0.4	90.8	-2.3

V. EXTRACTION OF SPECTRAL COMPONENTS: GLOBAL FIT OF KINETIC TRACES

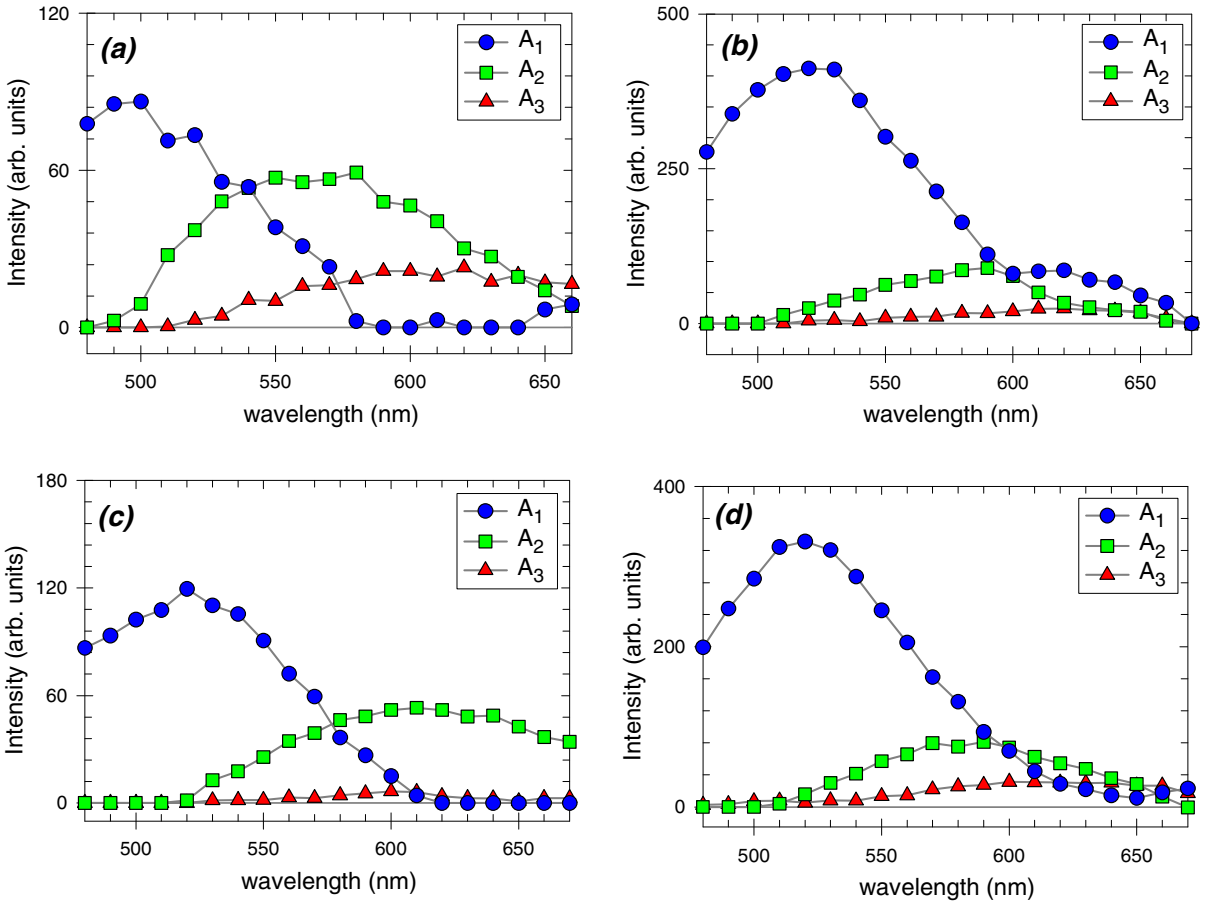

Figure S6. Pre-exponential factors A_1, A_2 and A_3 obtained by means of a global fit of eq. 1 to time traces of luminescence intensity measured from the Etpy (a), Cl (b), Br (c), and I (d) complexes in CH_3CN. Luminescence signals were averaged over 10 nm intervals.

IV. EXTRACTION OF SPECTRAL COMPONENTS: SINGULAR VALUE DECOMPOSITION (SVD) AND GLOBAL FIT (GF) ANALYSIS

Our Fluorescence up-conversion data (Figure 2) represent a 2-variable measurement, where the luminescence intensity $E(\lambda,t)$ is measured as a function of wavelength and time delay. This corresponds to an M **x** N matrix, where M defines the number of wavelength points (in this case 256 discrete wavelength measurements each corresponding to a detector pixel) and N the number of time steps.

To minimize the number of spectra and time traces in the data, and to suppress the noise we first performed a singular value decomposition (SVD). This allows reducing the data

dimensionality and permits performing a nonlinear least square global fit on the reduced data, without losing any relevant information.

In the following, we give a brief description of the method tailored to the purpose of this article. In general, a time-resolved spectrum $E(\lambda,t)$ can be thought of as a superposition of the contributions of *P* different components:

$$E(\lambda,t)=\sum_{l=1}^{P}E_l(\lambda,t)+\Xi(\lambda,t)=\bar{E}+\Xi$$

where the $\bar{E}$ matrix contains all the information about the spectral evolution of the system, whereas the Ξ matrix represents the stochastic normally-distributed noise with zero mean value. Without any *a priori* knowledge about the temporal evolution of these components we can assume that the each can be factorized:

$$\bar{E}(\lambda,t)=\sum_{l=1}^{P}\varepsilon_l(\lambda)c_l(t)$$

where $\varepsilon_l(\lambda)$ and $c_l(t)$ are the spectral distribution and the temporal evolution of the *l*-th component. This assumption means that the spectral evolution of each component as a function of time concerns the amplitude but not the band shape. Thus, the M x N data matrix is composed of discrete sets of wavelengths λ_i and time delay t_k :

$$E(\lambda_i,t_k)=\sum_{l=1}^{P}\varepsilon_l(\lambda_i)c_l(t_k)+\Xi(\lambda_i,t_k)$$

The SVD procedure allows to determine *P* as well as the M- and N-dimensional vectors $\varepsilon_l(\lambda_i)$ and $c_l(t_k)$, respectively, and to separate the stochastic noise contribution. It consists in decomposing the *E* matrix into a product of three components according to:

$$E=USV^T \qquad \text{(SI.1)}$$

where U and V^T stand for orthogonal matrices of M x M and N x N dimensions, respectively. Their columns contain the left and right singular vectors. In the case of Fl-UC data, the SVD approach yields U and V^T matrices, which we can identify as basis spectra and basis kinetic (time) traces, as shown in previous works.[3, 4] The diagonal elements of the S matrix yield the singular values $S_{ii}=s_i$.[5] With *P* components and noise-free matrix we should obtain $s_1>s_2>\ldots>s_P>s_{P+1}=0$. Even if the presence of Ξ perturbs the outcome of the SVD analysis, the comparison between the values of s_i allows to determine the number of components from the

number of singular vector pairs and accompanying singular values significantly different from noise.[1]

According to the scheme presented in the article, we assume a sequential relaxation, in which the temporal evolution of the system is described by:

$$V_i^T = \left\{ a_{i1} e^{\left(-\frac{t}{\tau_1}\right)} + a_{i2} \left[e^{\left(-\frac{t}{\tau_2}\right)} - e^{\left(-\frac{t}{\tau_1}\right)} \right] + a_{i3} \left[e^{\left(-\frac{t}{\tau_{ph}}\right)} - e^{\left(-\frac{t}{\tau_1}\right)} \right] \right\} \otimes e^{\left[-\left(\frac{t-t_0}{0.6*\Delta_{IRF}} \right)^2 \right]} \quad \text{(SI.2)}$$

where the first term corresponds to the state directly populated by the excitation pulse and decaying with τ_1; the second and third ones describe the two states indirectly populated from the first state with a rise-time τ_1 and decaying with τ_2 and τ_{ph} (tens of ns, herein assumed = ∞), respectively. The last Gaussian term describes the convolution with the instrument function (IRF), where Δ_{IRF} and t_0 are its FWHM and the time zero, respectively.

Within a GF analysis all significant V_i^T traces are simultaneously fitted in terms of Eq. SI.2, where the time constants have been considered as common (global) parameters. The coefficients $a_{i,k}$ are used to calculate the corresponding decay-associated spectra (DAS) of the involved kinetics by using the set of properly weighted U_i spectral SVD components via:[1]

$$DAS_{k=1,2,3} = \sum_{i=1}^{N} a_{i,k} \cdot s_i \cdot U_i \quad \text{(SI.3)}$$

The obtained DAS contain the contribution of corresponding lifetime decays τ_i in the spectral evolution of the system.

The SVD of the Fl-UC data set (Figure 2) was performed according to Eq. SI.1. It was followed by the global fitting of the kinetic V_i^T components retained after the transformation using the global fit function, defined in Eq. SI.2 . Once all the SVD kinetic components are fitted, using the extracted pre-exponential coefficients $a_{i,k}$, we have constructed the decay-associated spectra (DAS) corresponding to the characteristic lifetimes τ_i used in the fit (see Eq. SI.2). As previously pointed out, we assume no time-dependent changes of the spectral band shapes in our data.

The representative case of the SVD analysis of the data of [Re(I)$(CO)_3$(bpy)] is summarized in figure S7, where panels a) through d) present, respectively, the singular values retained in the analysis, their corresponding spectral U_i and temporal V_i^T basis sets together with the fitted curves using the aforementioned kinetic model, and the selected single-

wavelength kinetic traces of the unreduced data set fitted using the same kinetic model. To better point out the weight of each spectral basis to the spectral decomposition (see eq. SI.3), they are multiplied by the relative singular value (see panel (a)). We have limited the analysis to wavelengths longer than 470 nm to avoid possible artefacts from the presence of the solvent Raman peak.

The analysis resulted in three dominant SVD components. Their spectral and kinetic parts are shown in figure S7c, respectively. To extract from them the spectral distribution of each involved state (see scheme I in the article) we calculated the DASs accordingly to eq. SI.3. In figure S8, we show them for all the samples (panel (d) shows the same results as Fig. 5 in the article). The all show a broad band at ~530 nm decaying with τ_1; an intermediate band at 570-620 nm associated to τ_2, and the weakest and red-most trace corresponding to the phosphorescence ($\tau_{ph} = \infty$).

According to the model proposed in the article (see scheme I and related discussion) the first component corresponds to the fluorescence from the directly populated, first excited singlet b^1A' state; the second and third components are populated from the singlet state and correspond to the emission from the third triplet b^3A'' and first triplet a^3A'' state emissions, respectively.

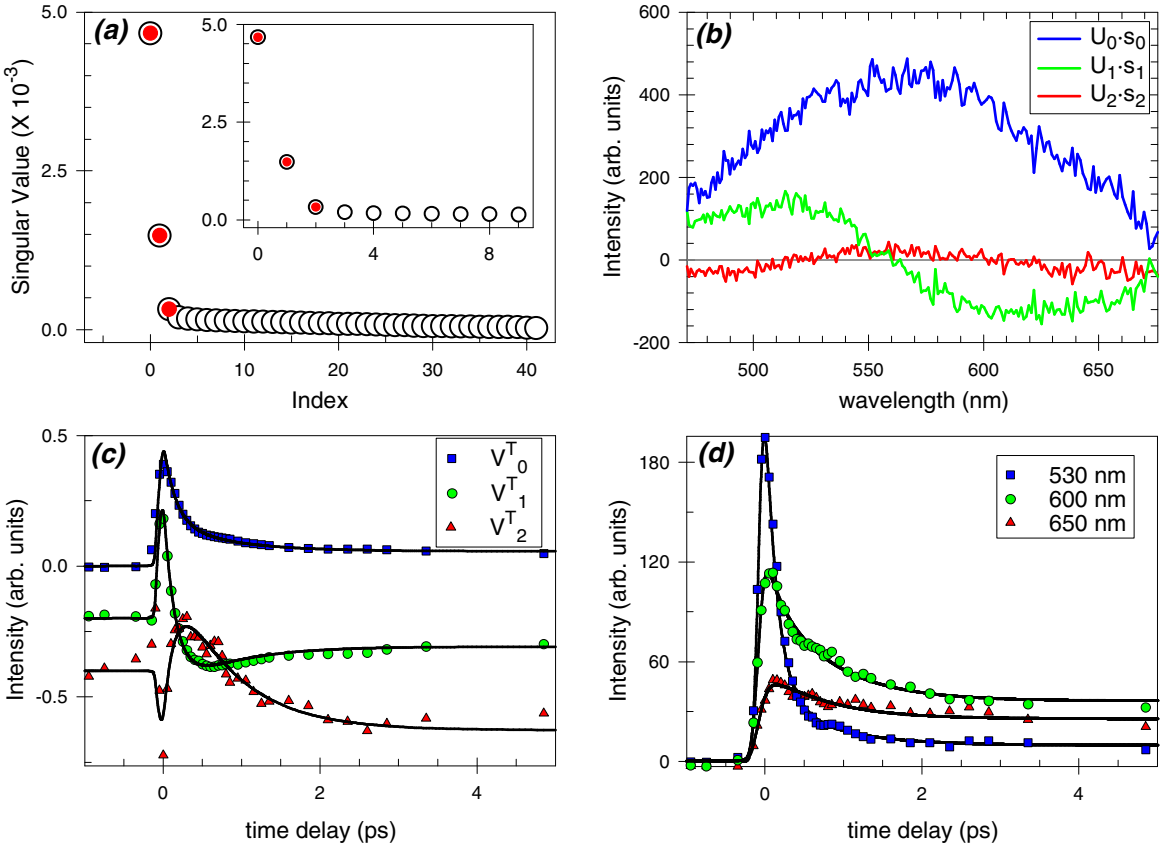

Figure S7. SVD decomposition of the fluorescence up-conversion data of [Re(I)(CO)$_3$(bpy)] in acetonitrile upon 400 nm excitation. Panel (a): singular values as obtained upon the decomposition (marks indicate the retained values), where the inset zooms into the initial 10 values to show better the noise cut-off of the singular values. Panel (b): spectral (U_i) basis vectors used in the data reconstruction multiplied by the relative singular value (see panel (a)). Panel (c) presents the temporal (V_i^T) basis along with the global fit results of the SVD kinetics (see eq. SI.2), for sake of clearness they are vertically shifted. In (d) the kinetic traces at 3 selected wavelengths are displayed together with their fits to the global kinetic model (eq. SI.2) discussed in the article (see Scheme I)

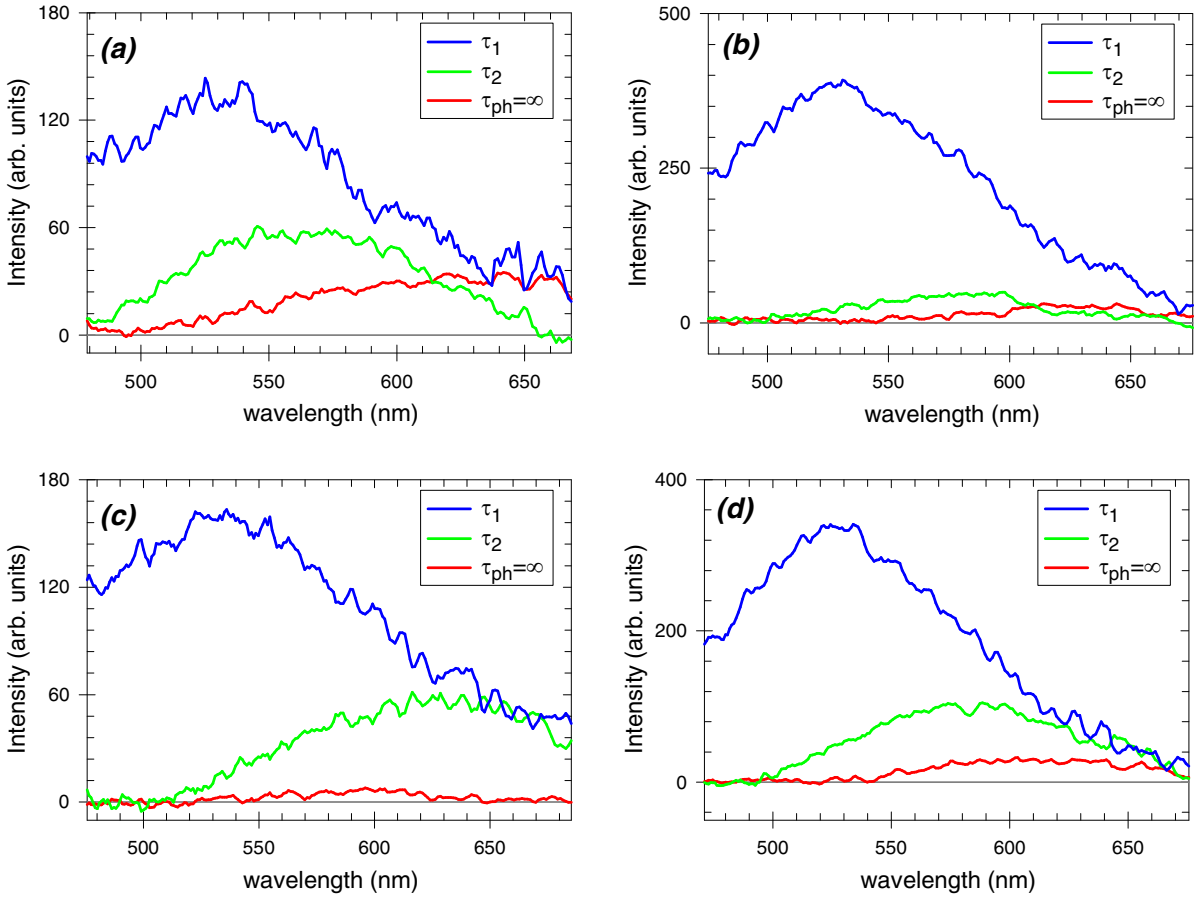

Figure S8. Decay Associated Spectra (DAS) for the Etpy-, Cl-, Br- and I-containing samples in acetonitrile (panel a) to d), respectively). Each panel shows three DASs which have been assigned to the luminiscence from the first excited singlet b^1A' state, the third triplet b^3A'' and the first triplet a^3A'', labelled τ_1, τ_2 and τ_{ph}, respectively (see Scheme I and relevant discussion in the article). We explicitly wrote $\tau_{ph} = \infty$ to stress that the third component correspond to a long-lasting phosphorescence.

References:

1. van Stokkum, I. H. M.; Larsen, D. S.; van Grondelle, R., Global and target analysis of time-resolved spectra. *Biochimica Et Biophysica Acta-Bioenergetics* **2004,** 1657, (2-3), 82-104.
2. Bonneau, R.; Wirz, J.; Zuberbuhler, A. D., Methods for the analysis of transient absorbance data. *Pure and Applied Chemistry* **1997,** 69, (5), 979-992.
3. Franzen, S.; Kiger, L.; Poyart, C.; Martin, J. L., Heme photolysis occurs by ultrafast excited state metal-to-ring charge transfer. *Biophysical Journal* **2001,** 80, (5), 2372-2385.
4. Helbing, J.; Bonacina, L.; Pietri, R.; Bredenbeck, J.; Hamm, P.; van Mourik, F.; Chaussard, F.; Gonzalez-Gonzalez, A.; Chergui, M.; Ramos-Alvarez, C.; Ruiz, C.; Lopez-Garriga, J., Time-resolved visible and infrared study of the cyano complexes of myoglobin and of hemoglobin I from Lucina pectinata. *Biophysical Journal* **2004,** 87, (3), 1881-1891.
5. Gampp, H.; Maeder, M.; Meyer, C. J.; Zuberbuhler, A. D., Calculation of Equilibrium-Constants from Multiwavelength Spectroscopic Data .1. Mathematical Considerations. *Talanta* **1985,** 32, (2), 95-101.

Complete references 20 and 22:

20. Frisch, M. J.; Trucks, G. W.; Schlegel, H. B.; Scuseria, G. E.; Robb, M. A.; Cheeseman, J. R.; J. A. Montgomery, J.; Vreven, T.; Kudin, K. N.; Burant, J. C.; Millam, J. M.; Iyengar, S. S.; Tomasi, J.; Barone, V.; Mennucci, B.; Cossi, M.; Scalmani, G.; Rega, N.; Petersson, G. A.; Nakatsuji, H.; Hada, M.; Ehara, M.; Toyota, K.; Fukuda, R.; Hasegawa, J.; Ishida, M.; Nakajima, T.; Honda, Y.; Kitao, O.; Nakai, H.; Klene, M.; Li, X.; Knox, J. E.; Hratchian, H. P.; Cross, J. B.; Bakken, V.; Adamo, C.; Jaramillo, J.; Gomperts, R.; Stratmann, R. E.; Yazyev, O.; Austin, A. J.; Cammi, R.; Pomelli, C.; Ochterski, J. W.; Ayala, P. Y.; Morokuma, K.; Voth, G. A.; Salvador, P.; Dannenberg, J. J.; Zakrzewski, V. G.; Dapprich, S.; Daniels, A. D.; Strain, M. C.; Farkas, O.; Malick, D. K.; Rabuck, A. D.; Raghavachari, K.; Foresman, J. B.; Ortiz, J. V.; Cui, Q.; Baboul, A. G.; Clifford, S.; Cioslowski, J.; Stefanov, B. B.; Liu, G.; Liashenko, A.; Piskorz, P.; Komaromi, I.; Martin, R. L.; Fox, D. J.; Keith, T.; Al-Laham, M. A.; Peng, C. Y.; Nanayakkara, A.; Challacombe, M.; Gill, P. M. W.; Johnson, B.; Chen, W.; Wong, M. W.; Gonzalez, C.; Pople, J. A. *Gaussian 03, Revision C.02*; Gaussian, Inc.: Wallingford, CT, 2004.

22. Ahlrichs, R.; Bär, M.; Baron, H. P.; Bauernschmitt, R.; Böcker, S.; Deglmann, P.; Ehrig, M.; Eichkorn, K.; Elliott, S.; Furche, F.; Haase, F.; Häser, M.; Horn, H.; Hättig, C.; Huber, C.; Huniar, U.; Kattannek, M.; Köhn, A.; Kölmel, C.; Kollwitz, M.; May, K.; Ochsenfeld, C.; Öhm, H.; Patzelt, H.; Rubner, O.; Schäfer, A.; Schneider, U.; Sierka, M.; Treutler, O.; Unterreiner, B.; von Arnim, M.; Weigend, F.; Weis, P.; Weiss, H., *TURBOMOLE V5-7*. Quantum Chemistry Group, University of Karlsruhe: Karlsruhe, Germany, 2004.